

Molecular Dynamic study of model two-dimensional systems involving Janus dumbbells and spherical particles

Ł. Baran, K. Dąbrowska, W. Rżysko, S. Sokołowski

Department for Theoretical Chemistry, Faculty of Chemistry, Maria Curie-Skłodowska University, Lublin 20-031, Poland

Received June 17, 2020, in final form May 25, 2021

We have performed an extensive constant temperature Molecular Dynamics study of two-dimensional systems involving Janus dumbbells and spherical particles. Janus dumbbells have been modelled as two spheres, labeled 1 and 2, joined together via harmonic bonds. Sphere 1 of a selected Janus dumbbell attracts the spheres of the same kind on other Janus dumbbells, while the interactions between the pairs 1-1 and 1-2 were repulsive. On the other hand, the spherical particles are attracted by centers 2 and repelled by the centers 1 of Janus particles. We have shown that the structure of oriented phases that can be formed in the system depends on the bond length of Janus dumbbells and the ratio of the number of spherical particles to the number of Janus dumbbells in the system. The presence of spherical particles is necessary to develop oriented phases. For the assumed model, the formation of oriented phases in the system depends on the concentration of spherical particles. Equal numbers of Janus and spherical particles create optimal conditions for the formation of lamellar phases.

Key words: *monolayers, mixture of Janus dumbbells and spheres, lamellar phases, molecular dynamics, structural properties*

1. Introduction

Particles of anisotropic shape and interactions play a significant role in the development of different self-assembling structures [1–3]. The self-assembly of these particles, which are often called as the “building blocks”, has now emerged as a versatile platform for the creation of novel materials with requested properties. These new materials have found numerous applications in science, medicine, biotechnology, for the production of photonic crystals, detection of biomolecules, energy harvesting and in many other fields [4–13]. On the other hand, the investigation of self-organization processes has also led to significant progress in the preparation and design of anisotropic particles of precisely defined size, shape, and functionality.

Janus particles that are composed of two or, in some cases, of a greater number of chemically distinct parts, constitute a unique class of anisotropic particles. Among different types of Janus-like particles, the so-called Janus dumbbells that are built of two jointed spheres of different chemical character are one of the simplest “building blocks” and have received much attention recently. In particular, the behavior and self-assembly of Janus dumbbells in bulk two- and three-dimensional phases, as well as at different interfaces have been extensively studied using computer simulations and theoretical approaches, e.g., density functional methods [14–22]. Theoretical methods for the description of the systems of anisotropic nanoparticles are similar to the methods used in the studies of systems involving amphiphilic molecules, e.g., surfactants, or even to some extent, of dipolar molecules [23, 24].

The conditions of self-organization and morphology of emerging phases formed by anisotropic nanoparticles depend on the presence in the system of other, usually spherical species [25–30]. Similar effects to those observed for nanoparticles have also occurred on molecular length scales, namely in

the case of formation of supramolecular structures in mixtures involving anisotropic and spherical molecules [31, 32]. In both cases, i.e., for nanoparticles, and for molecules organizing into supramolecules, the properties of self-assembled structures depend on the system composition and on the ratio of sizes of the involved components. Careful tuning of these parameters can enable directing the system self-assembly toward architectures with predefined morphology and functions.

Self-assembling nanoparticles are dissolved in an inert solvent that does not directly participate in the resulting structures. The main problem with accurate modelling of those systems at a microscopic level is connected with the difference in sizes between nanoparticles and solvent molecules. In experimental setups, the size of nanoparticles is usually bigger than 100 nm, i.e., the size of nanoparticles is at least a few hundred times greater than the size of the fluid molecules. Such a large difference can be handled using thermodynamic approaches that are based on macroscopic quantities such as surface and line tensions, but then the microscopic structure of the system is neglected [33, 34]. In the case of computer simulation that is focused on a detailed description of the microscopic structure, the difference in sizes between fluid and nanoparticles should be much smaller. In fact, in the existing publications, the size of simulated nanoparticles has ranged from a few to a dozen or so diameters of the fluid solvent molecules [35–38]. Thus, the simulated nanoparticles were at least ten times smaller than in experimental systems.

One of the possible methods of simulating systems containing nanoparticles is the use of the so-called implicit solvent models [39, 40]. According to these models, the presence of solvent molecules is neglected. The interactions between all remaining species are treated as being “effective” or solvent-mediated. The term “effectiveness” means that the interaction potentials take into account the presence of solvent molecules in an implicit way. The implicit solvent models are computationally efficient and can provide a reasonable description of the self-organization effects.

The main focus of the present study is on the presentation of the simulation results of the development of self-organized phases in two-dimensional systems involving Janus dumbbells of different elongation and different concentrations of spherical particles. We want to study how the two factors, namely, elongation of dimers and concentration of spherical particles, affect the formation of self-assembled structures. The systems are modelled within the implicit solvent model. The structural properties of investigated mixtures have also been contrasted with the properties of systems involving Janus dumbbells alone. The systems of homo- and heteronuclear dimers of different elongation have already been investigated in numerous works [41–46], but the models of interactions used in the above-cited publications differ from those used by us.

We employ Molecular Dynamics simulations to investigate the occurrence of ordered phases at different concentrations of spherical particles and at different temperatures. However, the aim of the work is not to determine the complete phase diagrams, but rather to draw attention to the possibility of the formation of different structures under selected conditions. The studies of similar mixtures have already been carried out [47–49], but they concentrated on the aggregation of colloidal spheres mediated by Janus dimers.

The paper is organized as follows. In the following section (section 2) we present the model. Then, the simulation method (section 3) is outlined. In section 4 we discuss the obtained results, starting from the systems in which the Janus dumbbells are built of two tangentially jointed spheres and different amounts of spherical particles. Next, we proceed to systems with shorter Janus dimers. Finally, we consider systems involving only Janus particles, without the spherical ones. The latter systems resemble those studied by Bordin and Krott [18, 19]. The main results are concluded in section 5.

This work is dedicated to Yuri Kalyuzhnyi, a distinguished scientist in the field of statistical thermodynamical theory of liquids, on behalf of his 70th birthday. We highly appreciate his friendship during the last decades and we would like to thank him for many interesting and fruitful scientific discussions.

2. Model

We consider systems involving either pure Janus dumbbells or mixtures of Janus dumbbells and spherical (circular) particles. Each Janus dumbbell is built of two jointed spheres of the same diameter, σ , located at a distance d apart. The atoms constituting Janus dumbbells are distinguished by the indices 1 and 2, whereas the index 3 refers to spherical particles.

The binding between atoms 1 and 2 is ensured by the harmonic potential

$$U_b(r) = k_H(r - d)^2, \quad (2.1)$$

where k_H is a constant. The interactions between all pairs ij , ($i, j = 1, 2, 3$), are described by the potential

$$u_{ij}(r) = \begin{cases} \Phi_{ij}^{(I)}(r) - \Phi_{ij}^{(I)}(r_{ij,c}) - (r - r_{ij,c}) \frac{d\Phi_{ij}^{(I)}(r)}{dr} & r \leq r_{ij,c} \\ 0, & r > r_{ij,c}, \end{cases} \quad (2.2)$$

where

$$\Phi_{ij}^{(I)}(r) = 4\varepsilon_{ij}[(\sigma_{ij}/r)^{12} - (\sigma_{ij}/r)^6]. \quad (2.3)$$

This potential combines the standard Lennard-Jones(12, 6) function and subtracts a linear term based on the cutoff distance, $r_{ij,c}$, so that both, the potential and the force, tend continuously to zero at the cutoff [52]. In the above, ε_{ij} and $\sigma_{ij} = 0.5(\sigma_i + \sigma_j)$ are the energy and the size parameters for the interactions between the pairs of the type i and j . The Lennard-Jones sizes of the atomic species 1 and 2 were equal, $\sigma_1 = \sigma_2 \equiv \sigma$, and σ was used as the length unit. The unit of the energy, however, was $\varepsilon_{22} \equiv \varepsilon$. The size of the particles 3 was two times smaller than σ , $\sigma_3 = \sigma/2$. The diameter σ_3 was ad hoc selected, though it is similar to that used in [47, 48].

The reduced quantities are distinguished by asterisks, i.e., $d^* = d/\sigma$, $\sigma_i^* = \sigma_i/\sigma$ and $\varepsilon_{ij}^* = \varepsilon_{ij}/\varepsilon$, thus $\sigma_3^* = 0.5$. The reduced temperature is defined as usual, $T^* = k_B T/\varepsilon$ where k_B is the Boltzmann constant.

If the cut-off distance equals $r_{ij,c} = 2^{1/6}\sigma_{ij}$, then the interaction potential is entirely repulsive [53, 54]. According to the assumed model, the attractive interactions exist only between the pairs 11 and 23. In other words, the attractive forces exist only between attractive parts of Janus particles and the repulsive parts of Janus particles and spherical molecules. All the remaining interactions are repulsive. The energy parameters, together with the cut-off distances are collected in table 1.

Table 1. The values of the parameters of equations (2.2) and (2.3).

ε_{11}^*	ε_{22}^*	ε_{33}^*	ε_{12}^*	ε_{13}^*	ε_{23}^*	$r_{11,c}^*$	$r_{23,c}^*$	$r_{22,c}^*$	$r_{12,c}^*$	$r_{13,c}^*$	$r_{33,c}^*$
4	1	1	1	1	4	1.6	$1.6\sigma_{23}^*$	$2^{1/6}$	$2^{1/6}$	$2^{1/6}\sigma_{13}^*$	$2^{1/6}\sigma_{33}^*$

The depth of the attractive well of the Lennard-Jones energy $u_{11}(r)$ is the same as for the pair of particles 2 and 3. Instantaneously, the particles 3 are smaller than the centers 1 and 2. Therefore, under certain conditions we can expect the formation of structures with the ‘‘building blocks’’ involving particles 3 (cf. reference [44]). To speed up the simulations, the range of all attractive interactions has been assumed to be short.

The model investigated by us does not describe any specific experimental setup. Similarly to the works [43–46] we aimed at finding sets of parameters for which the development of interesting structures could be observed. Before selecting the values of the parameters from table 1, we carried out several auxiliary short simulation runs.

We stress that the harmonic bonding potential constant [cf. equation (2.1)] was $k_H/\sigma^2 = 1000\varepsilon$. A high value of this constant ensures very small harmonic vibrations of the length of Janus dumbbells bonds.

3. Simulation details

The simulations were carried out using the LAMMPS package [55]. The in-plane, OXY , cell dimension was $L \times L$ and the periodic boundary conditions were applied. The numbers of Janus dumbbells and spherical particles are designated as N_J and N_3 , respectively. The system initial composition is given in

terms of the ratio $\chi = N_3/N_J$. The numbers N_J and N_3 , as well the ratio χ always refer to the nominal values, averaged over the entire system.

To model the particles immersed in an implicit solvent, a Langevin thermostat was employed. The masses of all atomic components were set to 1. The Langevin thermostat is weakly coupled to the system, the dumping constant in the LAMMPS input file [56] was 10. Since the aim of the simulations was to study the systems at equilibrium, the selection of masses of the particles was irrelevant.

The reduced time step, $\tau = t\sqrt{\varepsilon/m\sigma^2}$ (where t is the time step in seconds), was $\tau^* = 0.001$. The choice of τ^* is a compromise between the time and accuracy of simulations. Our selection of τ^* resulted from the performed tests. Unfortunately, during simulations, we determined only the values of S .

Before performing the final runs, we considered different possibilities for selecting the order parameter that can be easily computed in simulations and decided to select the nematic order parameter of S . We modified the description of equation (3.1) and the description of the results. We also added several references related to this problem.

A great majority of the results are for $N_J = 900$, but to verify the obtained results, several calculations were also performed for $N_J = 1800$. The total number of simulated spherical entities was $2N_J + N_3 = 2N_J + \chi N_J$.

In the forthcoming discussion, the nominal system density is given by the total packing fraction. It is defined as $\rho^* = (N_J V_J + N_3 V_3)/V_{\text{box}}$, where $V_J = \pi\sigma^3/3 - \pi(2\sigma + d)(\sigma - d)^2/12$ is the volume of the Janus dumbbell, V_3 is the volume of a spherical particle and $V_{\text{box}} = L^2\sigma$.

We carried out equilibration runs for 5×10^7 time steps and after that time the production steps were continued until sufficient statistics for the measured properties were reached. At the initial stage of equilibration, the nominal density of every system ρ^* was adjusted by short NPT runs during which the size of the simulation cell was varied. After that, the size of the cell and thus the nominal system density, ρ^* , were kept constant during consecutive NVT simulation.

The purpose of the simulation was to coarsely determine the phase diagrams using the method of block density analysis. Our calculations were carried out for the nominal values of χ equal to $\chi = 1, 2$ and 4.

The values of ρ^* were selected in such a way that they were approximately equal to the average density of the coexisting phases at the lowest temperature. The selection of specific values of ρ^* was made by conducting preliminary NVT simulations for various nominal densities.

The formation of ordered phases can result in different numbers of particles of different kind and different compositions in some parts of the systems. In the forthcoming discussion, the symbols ρ_L^* and χ_L refer to distinguished parts (phases) of the system.

To characterize the systems, the following structural characteristics were evaluated:

- i. radial distribution functions between the species 1, 2, 3 and the radial distribution function between centers of mass of Janus dumbbells, particles,
- ii. the distribution of cluster sizes formed by Janus dumbbells,
- iii. the order parameter for characterizing the orientational ordering of Janus dumbbells.

From the center of mass radial distribution function, the distance that corresponds to its first minimum, $R_{JJ,m}$, was estimated. This distance was in turn used to calculate the cluster size distributions using the algorithm of Rapaport [57].

The development of ordered structures in the systems under study resembles the behavior of liquid crystals. The order in liquid crystals can be studied by introducing different order parameters [58, 59], as well as the complex positional order parameters [60]. Since the analysis of preliminary data indicated the appearance of lamellar phases under certain conditions, we decided to characterize the changes of the orientational ordering of Janus dumbbells by the tensor order parameter. Its definition is given in the work of Eppenga and Frenkel [61]. It reads

$$Q_{\alpha\beta} = \frac{1}{N_J} \sum_i^N [2b_\alpha(i)b_\beta(i) - \delta_{\alpha\beta}]. \quad (3.1)$$

In the above, $b_\alpha(i)$ [$b_\beta(i)$] is the α -th (β -th) coordinate of the unit vector \mathbf{b} , specifying the orientation of the molecule i , and $\delta_{\alpha\beta}$ is the Kronecker delta function. \mathbf{Q} is a traceless symmetric second rank tensor, with three eigenvalues λ_+ , λ_0 , λ_- . The nematic order parameter S is defined as the largest positive eigenvalue, λ_+ . S takes on the values between 0 and 1 and equals 0 in completely disordered phases and equals 1 in perfectly ordered phases, respectively [61].

4. Results and discussion

The principal aim of our study was to investigate the changes in the structure of the system with the change of the length of Janus dumbbells and with the composition of the system. We begin our discussion with the presentation of the results for the systems involving Janus dumbbells (of the bond length $d^* = 1$) and spherical particles at three nominal concentrations, $\chi = 1, 2$ and 4. The calculations were carried out at several temperatures from the range $0.2 \leq T^* < 0.5$. The total nominal system density was adjusted to $\rho^* = 0.217$.

At low temperatures, the system splits into two subsystems. One of them contains a single, big “cluster” of lamellary ordered particles, while the second involves extremely rarefied, gas-like phase. In figure 1a we show a part of the lamellar structure that was formed at $T^* = 0.2$. Note that for the assumed cut-off distances of the interaction potentials, the structural ordering in the system is expected to appear at quite low temperatures.

The lamellar morphology of the dense phase (figure 1a) results from the attractive interactions in the system, especially from the attraction between pairs 2 and 3. Bilayers of dumbbells that are formed due to attractive interactions between centers “1” are “glued” together via spherical particles attracted by repulsive parts of the Janus dumbbells. The spherical particles form one-layer stripes and the entire structure consists of a staggered Janus bilayer and a single layer of spheres. The two-dimensional structure factor from figure 1b) perfectly captures the lamellar nature of the formed phase. Note that the two-dimensional structure factor was computed using the method outlined in our previous work [30].

At $T^* = 0.2$, almost all the particles in the system are involved in the formation of the lamellar phase. Only incidentally some single particles of both kinds have appeared outside this phase, indicating that the gas phase density in equilibrium with the lamellar phase is almost zero. The nominal reduced density of the lamellar phase evaluated from the block analysis [62] is $\rho_L^* = 0.425 \pm 0.08$ and its composition is the same as the assumed starting composition, $\chi_L = 1$.

We have checked that the lamellar phase exits up to $T^* \approx 0.35$, while at higher temperatures, the system becomes a disordered, mixed fluid. Examples of the snapshots illustrating the temperature evolution of the system are shown in the Appendix, cf. figure A.1. In this Appendix, we also enclosed the plot of the two-dimensional structure factor (figure A.2) at $T^* = 0.4$ that corresponds to a fluid-like structure.

Figure 2a shows the dependence of the order parameter, S , on temperature. Up to $T^* \approx 0.35$, the values of S are almost constant, but at higher temperatures, they drop to zero indicating that the lamellar order disappears. Indeed, we observed that at temperatures higher than ≈ 0.35 the single lamellar cluster splits into several smaller ones. Figure 2b illustrates the temperature dependence of the density of dense and rarefied phases obtained from the block analysis. As in the case of the temperature dependence of S , the data resulting from the block analysis indicate that the separation of the system into two phases disappears at temperatures higher than ≈ 0.35 .

Figure 2c displays the distribution of the cluster sizes formed by Janus dumbbells at $T^* = 0.3$. The average cluster size is equal to $\langle N_c \rangle \approx 64$. The tendency to form clusters for the system with $\chi = 1$ vanishes at high temperatures, cf. the Appendix, figure A.3.

Finally, we show examples of the radial distribution functions between the attractive centers of Janus dumbbells, $g_{11}(r)$, and between spherical species, $g_{33}(r)$. The results are at two temperatures. At $T^* = 0.2$, the lamellar phase exits, while at $T^* = 0.4$ the system contains a mixed disordered fluid. At the low temperature of $T^* = 0.2$, both distributions point to the existence of the order in the system. Interesting is the shape of $g_{33}(r)$. The latter function exhibits “decaying periodic” character. The distance between consecutive periodically recurring patterns corresponds to the distance between consecutive one-layer stripes of spherical particles. The inner structure of each pattern results from localization of spherical

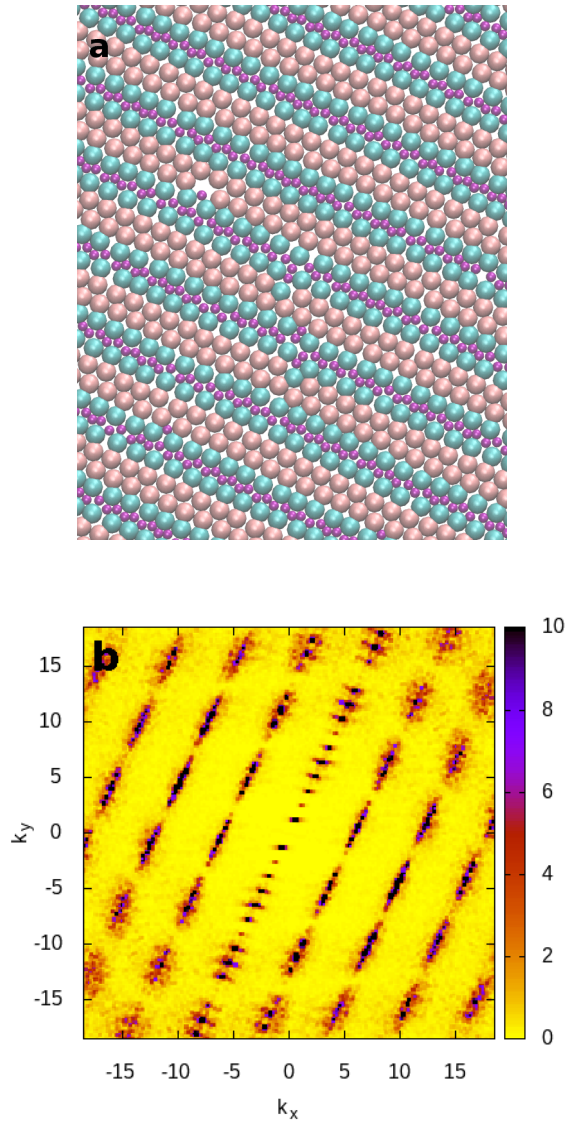


Figure 1. (Colour online) Panel a shows the snapshot of a panel of the lamellar phase and panel b — the two-dimensional structure factor obtained from $g_{11}(r)$. The calculations are at $T^* = 0.2$. The nominal density is $\rho^* = 0.217$ and $\chi = 1$. Pink and light blue spheres denote the attractive and repulsive parts of Janus dumbbells, while magenta spheres are the spherical particles.

particles within each stripe. At $T^* = 0.4$, however, the functions $g_{11}(r)$ and $g_{33}(r)$ are characteristic of a mixed, liquid-like phase.

We now proceed to the cases of systems with $\chi = 2$ and $\chi = 4$. The nominal densities in these systems were $\rho^* = 0.219$ and $\rho^* = 0.214$, respectively. In figure 4 we display the snapshots for both systems at $T^* = 0.2$.

For $\chi = 2$, the lamellar topography is still preserved at low temperatures (see figure 4a). However, the bilayers of Janus dumbbells and the strips of spherical particles do not run in parallel, but they bend over longer distances. This structure can be called “rippled lamellae” [18]. Although the values of the order parameter S (figure 5a) are now lower than for $\chi = 1$, the shape of the curves S vs T^* in figures 5a and 2a is similar and for temperatures lower than ≈ 0.35 only a single “rippled lamellae” exists in the system. The density of this phase (figure 5b) is lower than for the system characterized by $\chi = 1$ (cf. figure 2b). Thus, a higher amount of spherical particles leads to the “looser” packing of the dense phase.

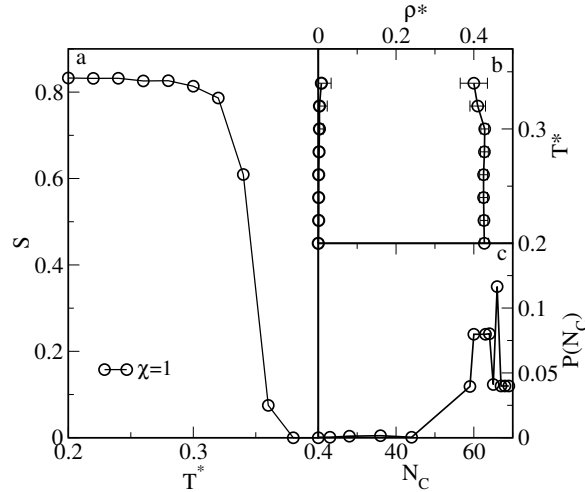


Figure 2. Nematic order parameter vs temperature (panel a), changes of the reduced density of dense and rarefied phases with temperature (panel b) and the distribution of the cluster sizes at $T^* = 0.3$ (panel c).

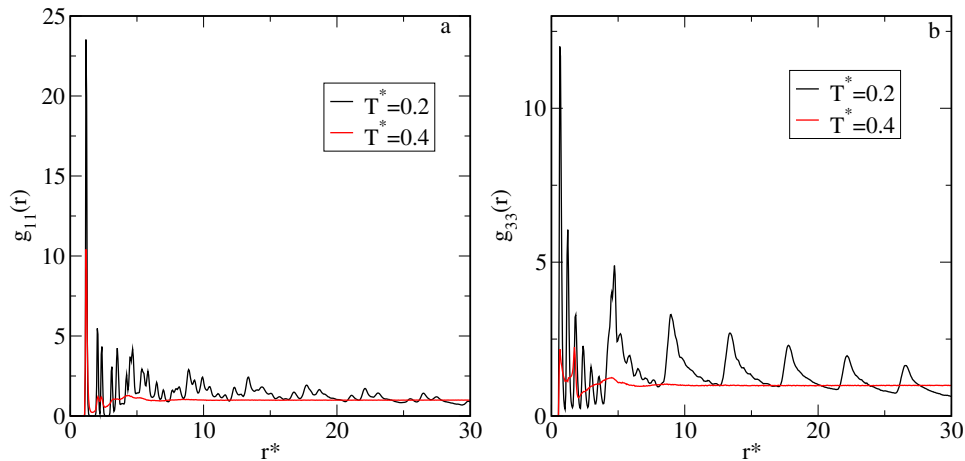


Figure 3. (Colour online) Radial distribution functions $g_{11}(r)$ (panel a) and $g_{33}(r)$ (panel b) at two temperatures, $T^* = 0.2$ and 0.4 . The nominal density is $\rho^* = 0.217$ and the nominal values of χ is 1.

Consequently, the distances between Janus particles increase and the cluster size (cf. figure 5c) decreases. The average cluster size for $\chi = 2$ is $\langle N_c \rangle \approx 11$, thus it is significantly lower than in the case of $\chi = 1$.

In the systems with $\chi = 2$, the total nominal number of spherical particles is two times higher than the nominal number of the Janus dumbbells. In the dense phases, the spherical particles try to surround the repulsive parts of Janus dumbbells. Since spherical particles appear in excess to dumbbells, the bilayers are twisting. Moreover, some spherical particles are released from the dense phase. Consequently, the rarefied phase consists almost exclusively of spherical particles. Figure A.4 in the Appendix provides additional insight into disaggregation of the initial large cluster in the system with $\chi = 2$. Pictures of the two configurations at temperatures of $T^* = 0.36$ and 0.38 are shown there. Despite the slight temperature difference, the configuration of the molecules at those two temperatures is completely different.

Our calculations have indicated that at $T^* = 0.2$, the composition of the dense phase, χ_L , (evaluated from block analysis) is $\chi_L \approx 1.91$. With temperature increase, the composition of the dense phase decreases slightly: at $T^* = 0.3$ it equals $\chi_L \approx 1.88$ and at $T^* = 0.34$ — $\chi_L \approx 1.84$.

For $\chi = 4$, the dense phase is still formed at low temperatures (figure 4b), but now it does not exhibit any lamellar order. The changes of liquid-like phase density with temperature is shown in figure 5b. The block data analysis has indicated that at temperatures higher than ≈ 0.31 the single liquid-like cluster

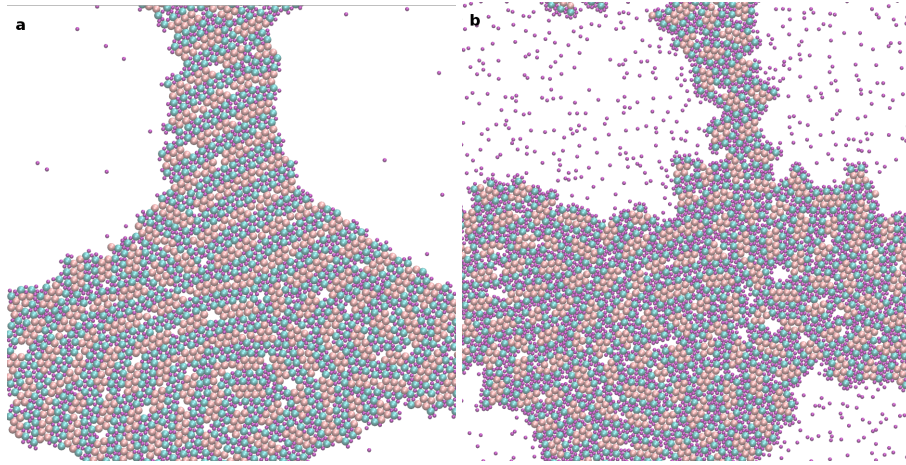


Figure 4. (Colour online) Snapshots of configurations in the systems with $\chi = 2$, $\rho^* = 0.219$ (panel a) and with $\chi = 4$ and $\rho^* = 0.214$ (panel b) at $T^* = 0.2$.

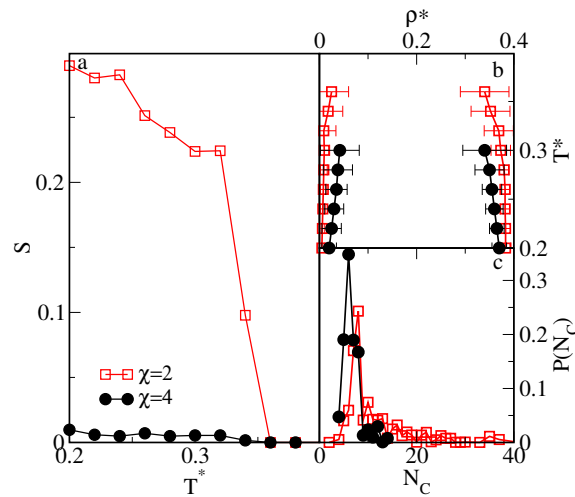


Figure 5. (Colour online) The order parameter S vs temperature (panel a), changes of the reduced density of dense and rarefied phases with temperature (panel b) and the distribution of the cluster sizes at $T^* = 0.4$ (panel c). The nominal densities ρ^* are 0.219 for $\chi = 2$ and 0.214 for $\chi = 4$.

is falling apart into several smaller ones. The mechanism of disaggregation is the same as outlined previously.

At lower temperatures, the single cluster composition, χ_L , is lower than the nominal value of χ and is equal to $\chi_L \approx 0.37$ at $T^* = 0.2$, $\chi_L \approx 0.36$ at $T^* = 0.24$ and $\chi_L \approx 0.34$ at $T^* = 0.3$. Similarly to $\chi = 2$, the coexisting rarefied fluid is composed mainly of spherical particles.

Figure 6 illustrates the changes of the average cluster size with temperature. Panel a is for the system with $\chi = 1$. In this case, the drop of $\langle N_c \rangle$ with temperature increase is the most pronounced and rapid. For the system with $\chi = 4$, the increase of temperature causes small changes in the cluster size. Of course, the values $\langle N_c \rangle$ depend on the selected cut-off distance, $R_{JJ,m}$. We recall that in our calculations this distance was equal to the distance of the first minimum of the radial distribution function for the Janus dumbbells.

At high temperatures, the structure of the systems with $\chi = 2$ and $\chi = 4$ is similar, cf. figure A.5 of the Appendix, where we enclosed snapshot of the configurations at $T^* = 0.5$. The radial distribution functions between all spherical species resemble the plots presented in figure 3 for the system with $\chi = 1$ at $T^* = 0.4$.

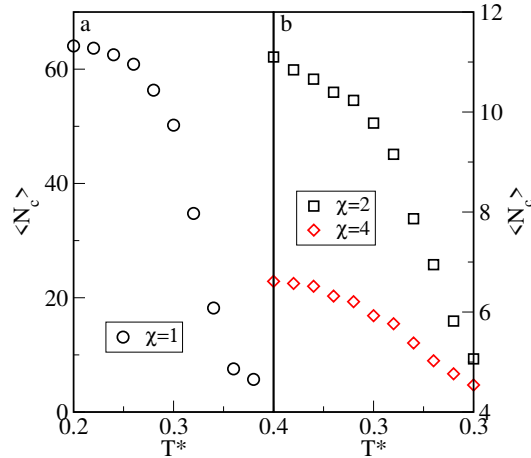


Figure 6. (Colour online) The dependence of the average cluster size $\langle N_c \rangle$ on temperature for the systems with $\chi = 1$ (panel a), $\chi = 2$ and $\chi = 4$ (panel b). The nominal density is 0.217 for $\chi = 1$, 0.219 for $\chi = 2$ and 0.214 for $\chi = 4$.

We now proceed to the system with $d^* = 0.5$. The two spheres forming Janus dumbbells do overlap. Similarly to $d^* = 1$, the calculations have been carried out for $\chi = 1, 2$ and 4.

For systems with $\chi = 1$ at low temperatures, only a single cluster composed of domains with non-zero values of the order parameter S appears, cf. figure 7a. Similar situation is observed up to $T^* \approx 0.36$, cf. figure A.6 in the Appendix. The main difference between the systems with $d^* = 1$ and $d^* = 0.5$ is the tendency to form differently oriented domains in the latter systems, whereas in the former systems a single cluster of equally oriented stripes usually appeared. We repeated the simulation for different starting configurations, and the tendency to form different domains was observed for all of them.

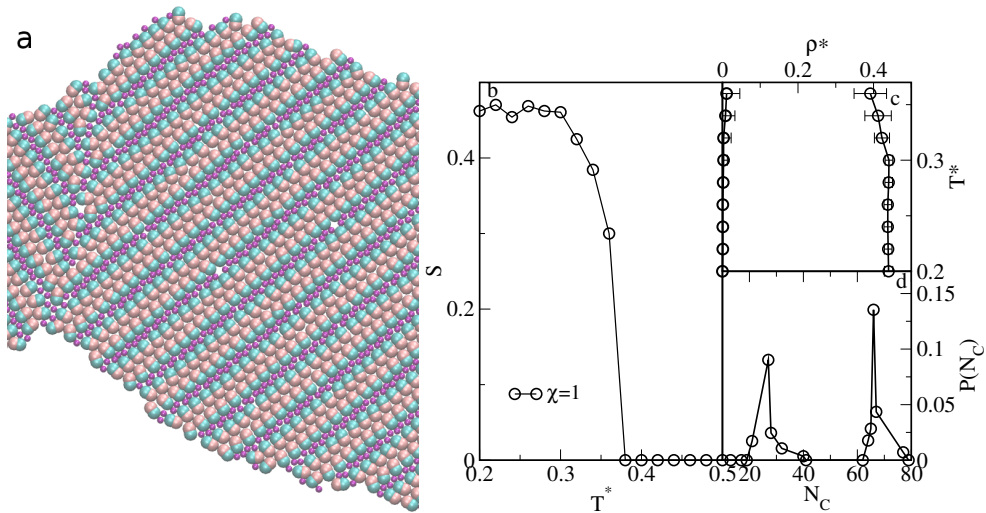


Figure 7. (Colour online) Panel a. The snapshot of the configuration for $\chi = 1, d^* = 0.5$ at $T^* = 0.2$. The symbols are the same as in figure 1a. Panel b illustrates the changes of the order parameter S with temperature. Panel c shows the changes of the densities of the coexisting phases with temperature and panel d displays the cluster size distribution at $T^* = 0.2$. The nominal system density was $\rho^* = 0.217$.

In figure 7b we present the relationship between the order parameter S and the temperature. The shape of the curve obtained for $d^* = 0.5$ is similar to that for $d^* = 1$, cf. figure 2a. However, the value of the order parameter S at a low temperature is almost two times lower than previously. This is connected with the existence of the domains mutually oriented at the angle of $\approx 90^\circ$.

The changes of the densities of rarefied and dense (lamellar) phases with temperature are shown in figure 7c. The density of the condensed phase is now slightly higher than for $d^* = 1$. Similarly to $d^* = 1$, the density of the rarefied phase is quite low. The gas-like phase consists of nearly equal amounts of spherical and Janus dumbbells. Thus, for systems characterized by $d^* = 1$ and $d^* = 0.5$, the nominal value of $\chi = 1$ seems to be optimal for the formation of ordered, lamellar phases.

Figure 7d displays the cluster size distribution $P(N_c)$. Two peaks of $P(N_c)$ are associated with the existing domains and for systems with $d^* = 0$ and $\chi = 1$, we also evaluated the radial distribution functions and the two-dimensional structure factors. Their overall shape and temperature behavior were quantitatively similar to the system with $d^* = 1$.

An increase of the content of spherical particles to $\chi = 2$ in the systems involving the dimers of elongation $d^* = 0.5$ leads to temperature changes similar to $d^* = 1$. An example of the configuration at a low temperature is shown in the Appendix, cf. figure A.7. At low temperatures, the clusters, mainly composed of 6, 7, 8, or 9 Janus dumbbells, are surrounded by spherical particles. These clusters built larger entities, in which they are oriented in parallel to each other. Particular larger entities are connected via spherical particles.

For $\chi = 2$, the number of spherical particles is evidently too large compared to the number of Janus dumbbells and even at the lowest investigated temperature, $T^* = 0.2$, several of them remain outside the big cluster of a dense phase. After inspecting several system configurations, we decided not to perform a detailed analysis of this case.

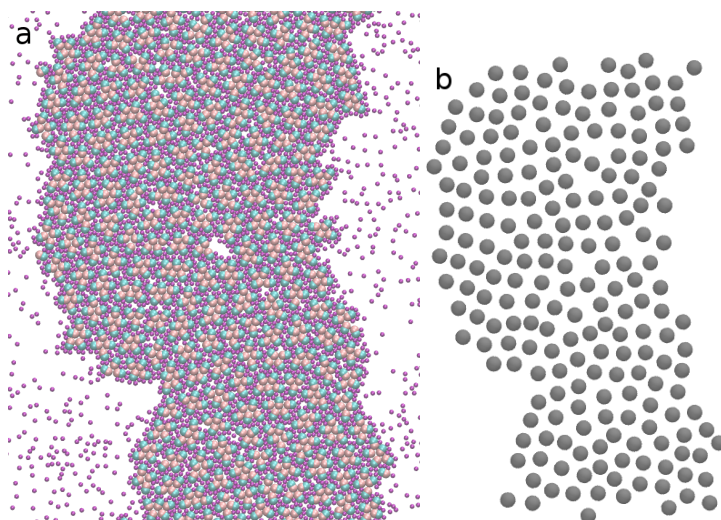


Figure 8. (Colour online) Snapshot (panel a) and the configuration of centers of mass of “elementary clusters” (panel b) for the system with $d^* = 0.5$, $\chi = 4$, at the nominal density $\rho^* = 0.211$ and at $T^* = 0.2$.

With a further increase of χ , the evolution of the structure of the system follows along the same lines as for $d^* = 1$. For $\chi = 4$, the dense phase is composed of clusters involving a small number of Janus particles (predominantly 4; we call them “elementary clusters”), separated by spherical ones, cf. the snapshot is shown in figure 4a. The size distribution of the clusters is presented in figure A.8a of the Appendix. We see here a single sharp peak at $N_c = 4$; there exist some clusters composed of 3 and 5, and, marginally, of 6 Janus dumbbells. The density of the condensed phase at $T^* = 0.2$ is $\rho^* \approx 0.38$ and its composition is $\chi_L \approx 0.38$. Both these values are somewhat higher than those estimated for the system with $d^* = 1$ (cf. figure 5b).

We have tried to inspect whether the centers of mass (COM) of “elementary clusters” are regularly distributed in the space. This point is illustrated in figure 4b, where we displayed the positions of COMs of particular clusters. By inspecting their configurations we can realize some traces of hexagonal ordering. However, the analyses of the radial distribution functions of COM, (cf. figure A.8b in the Appendix), as well as two-dimensional structure factors do not discover any pronounced hexagonal ordering. A dense

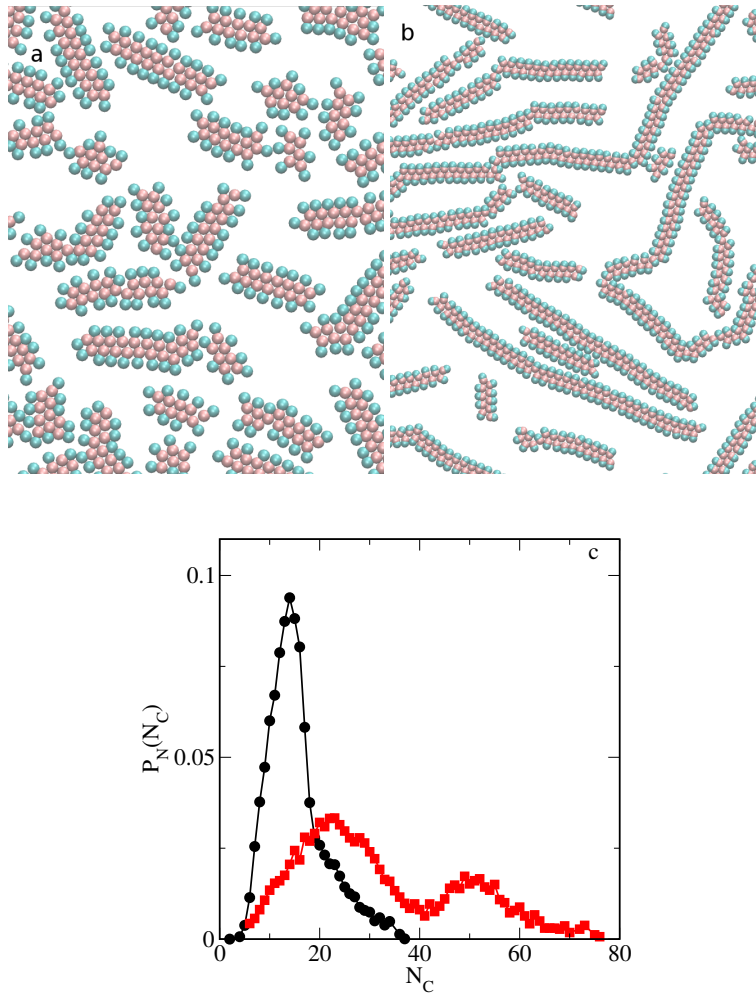


Figure 9. (Colour online) Snapshot for the system containing only Janus dumbbells. Panel a is for $d^* = 1$, while panel b for $d^* = 0.5$. Snapshots show only a part of the entire system. Panel c. The distribution of the cluster sizes for systems with $d^* = 1$ (black line and circles) and $d^* = 0.5$ (red lines and squares). The nominal density is 0.22 for both bond lengths d^* . The temperature is $T^* = 0.2$.

system behaves like a liquid of spherical particles with floating small “elementary clusters”.

Before proceeding further, we summarize the results obtained for mixtures involving Janus dumbbells of the lengths of $d^* = 1$ or $d^* = 0.5$ and spherical particles. In both cases, we observed the formation of lamellar structures. However, the appearance of the ordering of that type is connected with an appropriate composition of the system. We can say that only for $\chi = 1$, a pronounced lamellar ordering can exist at low temperatures. For any other composition, this ordering is, at least partially, destroyed by an excessive number of spherical particles, due to their attraction by the repulsive parts of Janus dumbbells. For shorter bonding distance, $d^* = 0.5$, this effect is more visible. However, one can ask whether the presence of spherical particles is necessary to create this ordering. To answer this question we carried out simulations of the systems containing dumbbell particles alone.

In figure 9 we show exemplary configurations of the systems at a quite low temperature of $T^* = 0.2$. For both elongations, i.e., for $d^* = 1$ (panel a) and $d^* = 0.5$ (panel b), we observe the formation of clusters. The dependence of the distribution of the cluster sizes is shown in figure 9c. The size of the clusters is smaller for $d^* = 1$, while for $d^* = 0.5$, elongated, spaghetti-like clusters appear. Note that the clustering observed in figure 9a resembles the one found in [18], for different interaction potential model.

It is also of interest that the clusters formed by shorter ($d^* = 0.5$) Janus dumbbells are partially ordered

in parallel, one relative to the other. Such an effect is not seen for longer ($d^* = 1$) Janus dumbbells. The existence of the partial directional cluster ordering is also reflected by the plot of the two-dimensional structure factor, cf. figure 4.

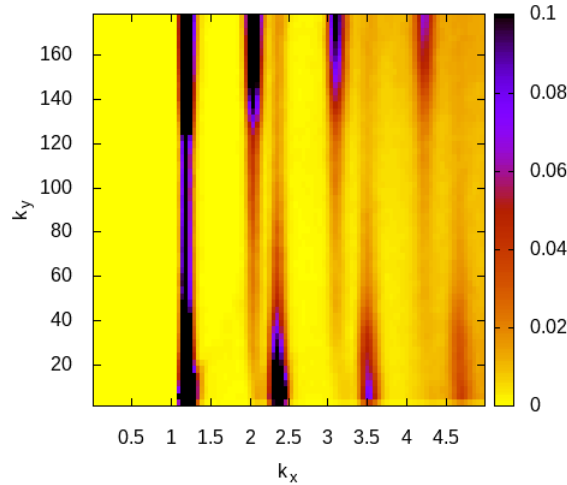


Figure 10. (Colour online) The two-dimensional structure factor for the system with $d^* = 0.5$. The nominal density is $\rho^* = 0.22$ and the temperature is $T=0.2$.

The formation of clusters results from the attraction between the centers 1 of Janus dumbbells. Preserving the geometry of Janus particles and, at the same time, decreasing the value of the cut-off distance $r_{11,c}^*$, we could observe the disappearance of the tendency to form clusters. The clusters exist since the Janus dumbbells are stuck together by attractive forces between their attractive parts. With temperature increase, the effect due to the attractive forces becomes less significant and the entropic effects lead to the breakup of long clusters into smaller parts, cf. figure A.9 in the Appendix.

Any attractive center of the Janus dumbbell located inside the cluster interacts with four attractive centers of other Janus dumbbells. Ideally, the axes of dumbbells would be oriented perpendicularly to the long axis of the cluster. Such an “ideal” configuration is easier to be realized by dumbbells with $d^* = 0.5$ than by more elongated dumbbells, since the repulsive parts of shorter Janus dumbbells are more effectively “locked” by repulsive potentials $u_{22}(r)$ and $u_{12}(r)$. Consequently, the clusters are longer for $d^* = 0.5$.

If long clusters are developed in the system, they can be treated as new entities, interacting each with the other almost exclusively via repulsive forces. The behavior of the system of such complex, elongated entities can be interpreted in terms of theories of liquid crystals [63]. At moderate densities, the parallel orientation of linear clusters is more favorable for long clusters. However, even at a quite low temperature, the clusters do not aggregate into bigger structures, due to the lack of attraction between them. Moreover, for possible development of a lamellar-like structure of clusters in the system involving only Janus dumbbells, the nominal density should be much higher than that used in our study.

By comparing the behavior of one-component and the mixed system, we can conclude that the lack of spherical particles prevents the formation of lamellar phases: there are no spherical particles sticking clusters together. Therefore, the presence of the spherical particles is necessary to observe transitions between disordered, liquid-like, and orientationally ordered, lamellar-type phases.

5. Conclusions

In this work we reported the results of Molecular Dynamics simulations of the systems involving Janus dumbbells and spherical particles. Janus dumbbells were built of two spheres, connected together by harmonic springs. Two bond length sizes were investigated. In the first model, the two spheres were tangentially jointed, whereas in the second model they partially overlapped. The spherical particles were two times smaller than the spheres building dumbbells. Our goal was to answer the following questions: (i) how the presence of spherical particles influences the self-organization of Janus particles and (ii) what is the mechanism of the formation of self-organized structures.

The calculations were carried out for a specific model, according to which the attractive forces exist between attractive parts of Janus dumbbells and between repulsive parts of Janus dumbbells and spherical particles. The forces between all remaining spherical components were repulsive. Moreover, the range of attractive interactions was small and, consequently, the changes in the structure of the system appeared within the range of quite low temperatures.

For systems containing Janus dumbbells and spherical particles, the existence of disordered and lamellary ordered phases was observed. The formation of lamellar phases was due to “gluing” bilayers composed of Janus particles by a single layer of spherical particles. Therefore, the presence of spherical particles is crucial for the development of lamellar structures. Indeed, this transition disappeared in the systems involving no spherical particles. On the other hand, in the case of mixtures, an excessive number of spherical particles causes the destruction of the lamellar structures.

For the highest investigated concentration of spherical particles, the formation of the orientationally ordered dense phase is suppressed and the dense phase consists of small clusters (preferably formed by four, five, or six Janus particles) “dissolved” in the fluid of spherical particles. We also checked that this phase does not exhibit any pronounced translational order. This finding is contrary to that found in [30] for mixtures of spherical Janus-like particles and spherical molecules.

The most pronounced lamellar ordering appeared in the systems containing equal amounts of Janus dumbbells and spherical particles, especially when both spheres forming Janus particles partially overlap (the length of Janus dumbbells is $d^* = 0.5$). This is undoubtedly connected with the assumed size of the spherical particles. For a larger difference of sizes between spheres forming Janus dumbbells and spherical particles, the ratio χ favoring the formation of ordered phases could be different.

As we have already stressed, an excessive number of spherical particles causes the destruction of the lamellar structures. For the highest investigated concentration of spherical particles, $\chi = 4$, we observed the development of a dense phase composed of small clusters (formed by four to six Janus dumbbells) “dissolved” in the fluid of spherical particles. However, the centers of mass of small clusters did not form any translational ordering. This behavior is contrary to that found in [30] for mixtures of spherical Janus-like particles and spherical molecules.

One could try to interpret the changes in the studied systems by analogy to the behavior of liquid crystals [63], using the following reasoning: if the two dumbbells “connected” together via attractive centers, are supplied with a spherical particle that can stick to the repulsive center of one dumbbell, then the formed entity can be treated as a new “building block”. This entity resembles a hard-rod-like particle and thus the behavior of the system should be similar to the behavior of hard-rod particles. However, this interpretation does not seem to be appropriate since, for liquid crystalline phases, the direction of long axes of rod-like particles determines the direction of the order. In our case, the angle between the direction of axes of dumbbells does not coincide with the direction of formed layers is non-zero. Moreover, the ordering is more pronounced for shorter dumbbells. Therefore, the explanation of the mechanism of the formation of liquid-crystalline ordered phases seems to be not appropriate for the description of the changes observed by us.

The model used by us is very simple. However, the mixture of asymmetric dimers and disks can also be employed as a model of amphiphilic molecules (e.g., surfactants) dispersed in an explicit solvent. In this case, realistic conditions would be those where the total packing fraction is liquid-like, and disks are more numerous and much smaller than dimers. In the near future, we plan to investigate the dynamics of self-assembly in our model, with specific attention to the nucleation and growth of lamellar structures.

Appendix

This Appendix contains additional figures illustrating the points discussed in the main text.

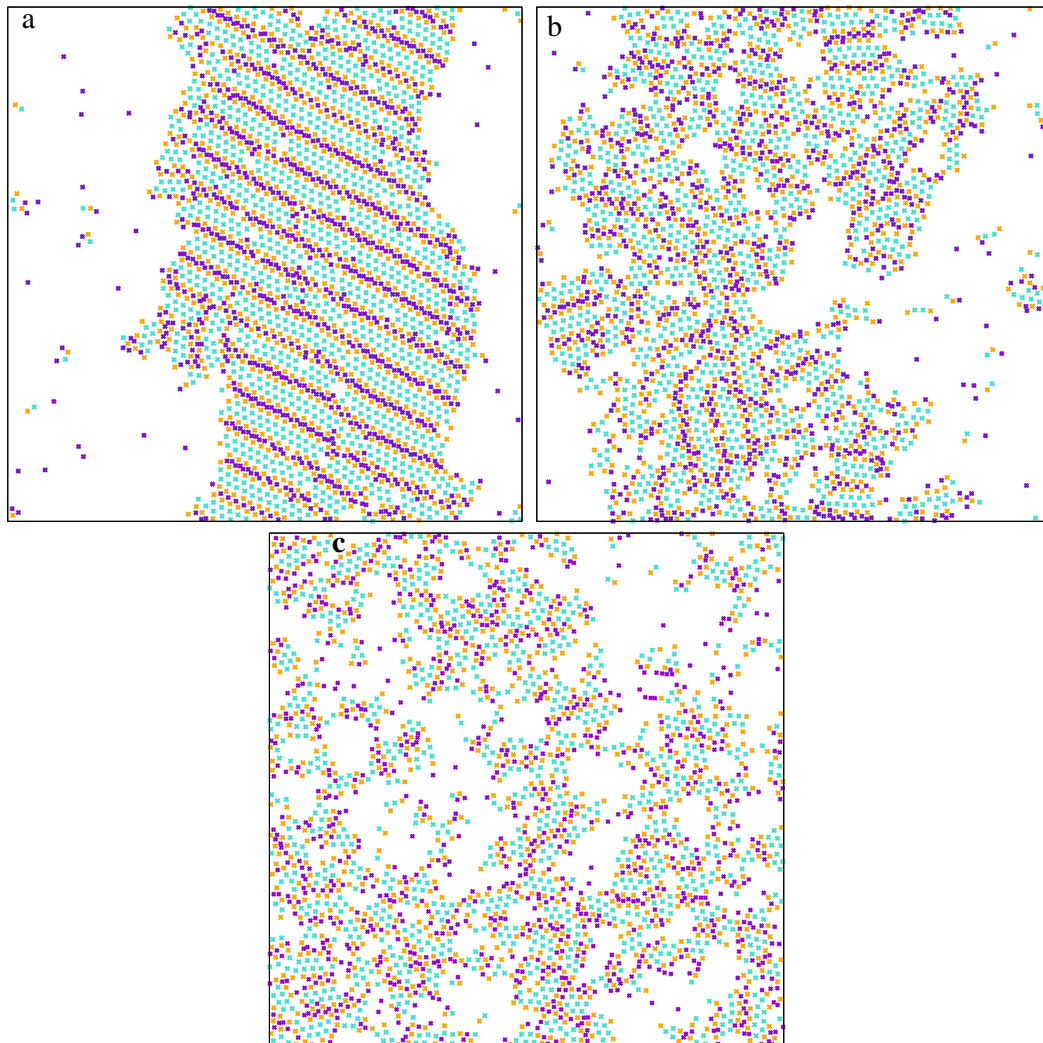


Figure A.1. (Colour online) Centers of all species in the system. Light blue and orange crosses are for attractive and repulsive Janus particles' components. Violet crosses are the centers of spherical particles. The calculations are for $T^* = 0.34$ (panel a), $T^* = 0.36$ (panel b) and $T^* = 0.4$ (panel c). The average reduced density of the entire system is $\rho^* = 0.217$.

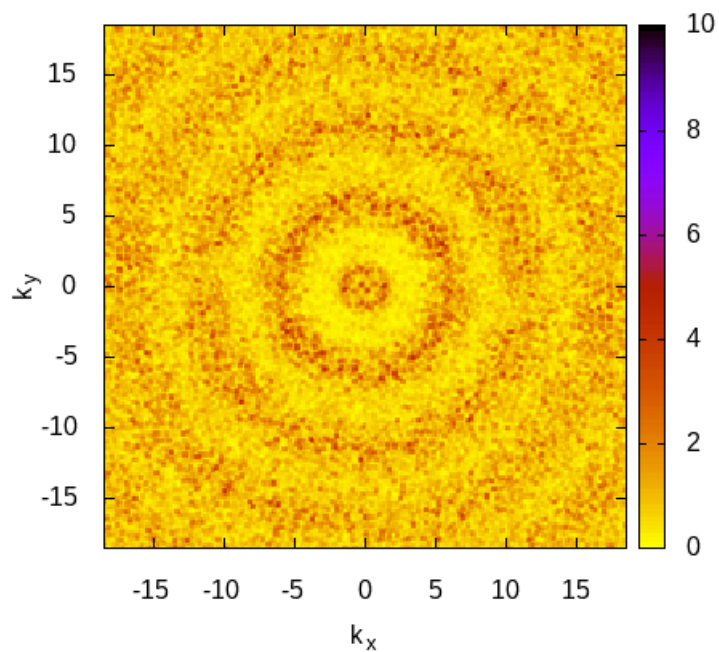


Figure A.2. (Colour online) Two-dimensional structure factor for the system at $T^* = 0.4$ and for $\chi = 1$ and $\rho^* = 0.217$.

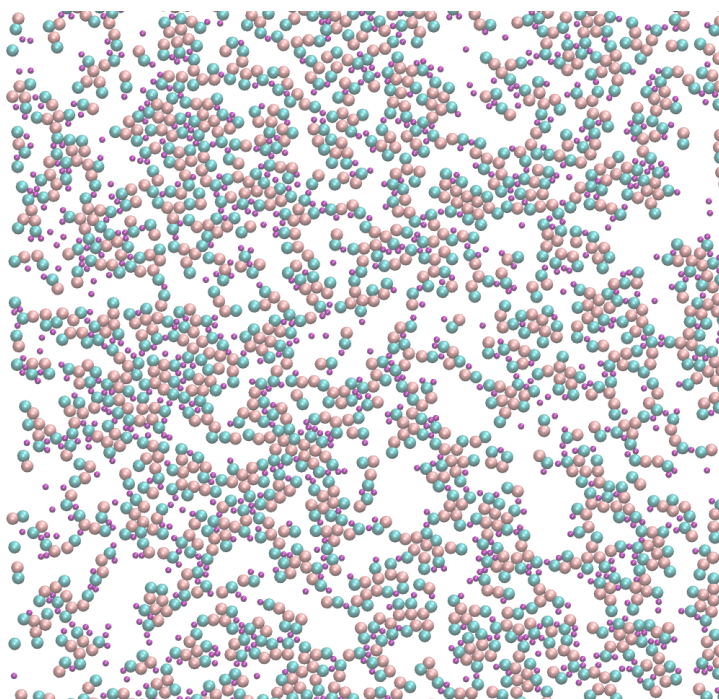


Figure A.3. (Colour online) The snapshot of the system with $\chi = 1$ at $T^* = 0.5$. The symbols are the same as in Figure 1a.

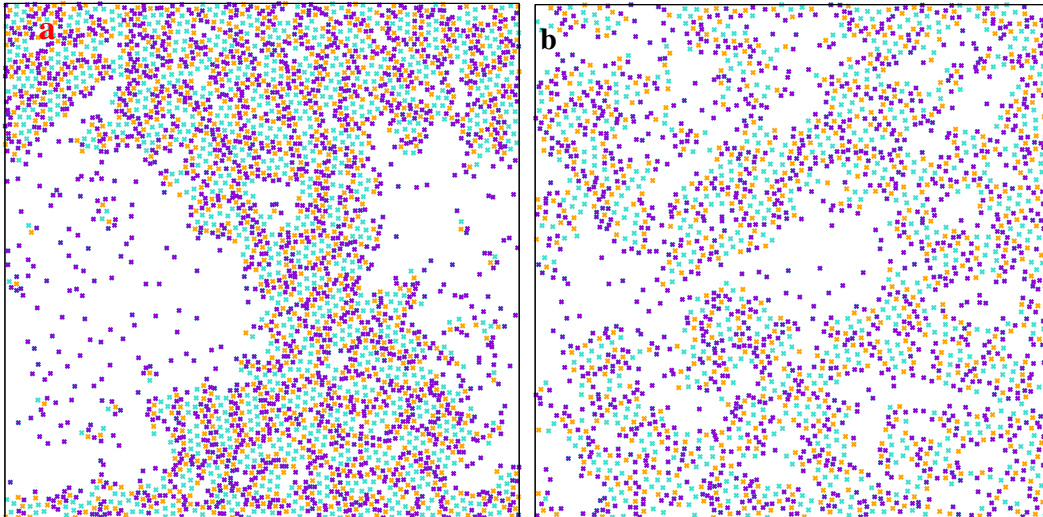


Figure A.4. (Colour online) Centers of all species in the system with $\chi = 2$. Light blue and orange crosses are for attractive and repulsive Janus particles' components. Violet crosses are the centers of spherical particles. The calculations are for $T^* = 0.36$ (panel a), and $T^* = 0.38$ (panel b). The average reduced density of the entire system is $\rho^* = 0.219$.

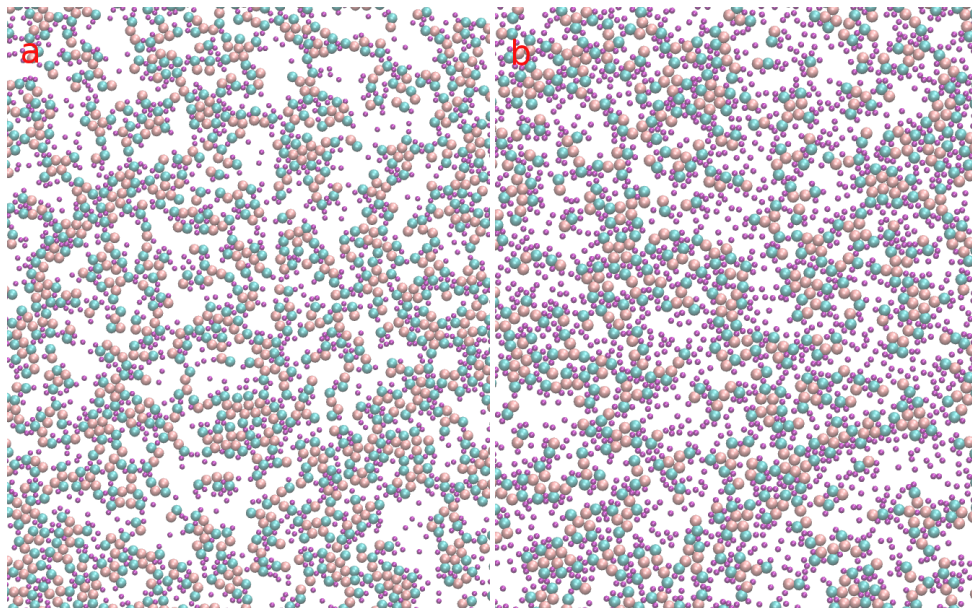


Figure A.5. (Colour online) The snapshots of the system with $\chi = 2, \rho^* = 0.219$ (panel a) and with $\chi = 4, \rho^* = 0.214$ (panel b). Color code is the same as in Figure 1a of the main text. The calculations are for $T^* = 0.5$.

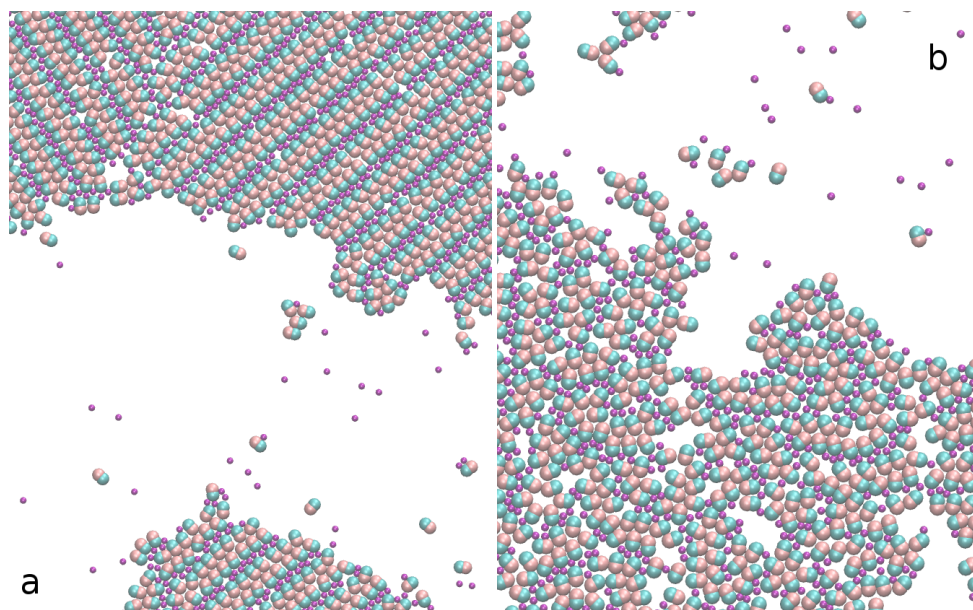


Figure A.6. (Colour online) Snapshots for the system with $d^* = 0.5$, $\chi = 1$ and the starting density of 0.217 at $T^* = 0.36$ (panel a) and 0.38 (panel b).

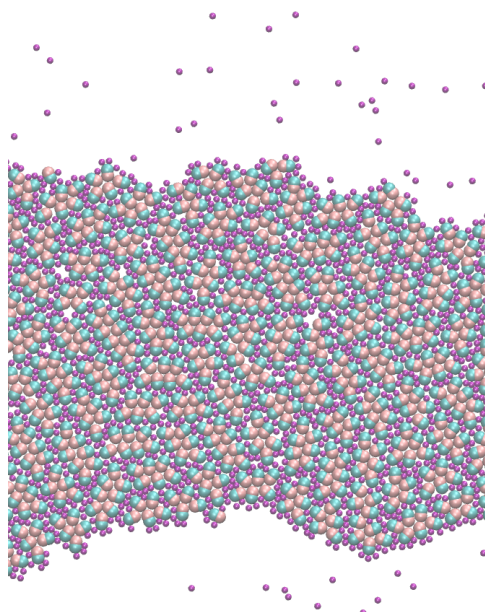


Figure A.7. (Colour online) Snapshot for the system with $d^* = 0.5$, $\chi = 2$ and the starting density of $\rho^* = 0.216$ at $T^* = 0.2$.

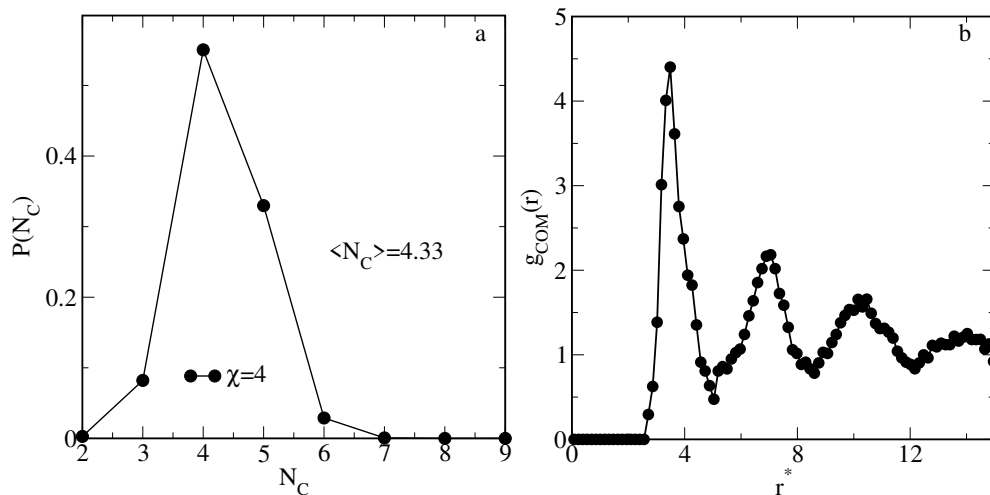


Figure A.8. Cluster size distribution (panel a) and the radial distribution function of the centers of mass of clusters (panel b) for the system with $d^* = 0.5$, $\chi = 4$ and $T^* = 0.2$. The starting density is $\rho^* = 0.211$.

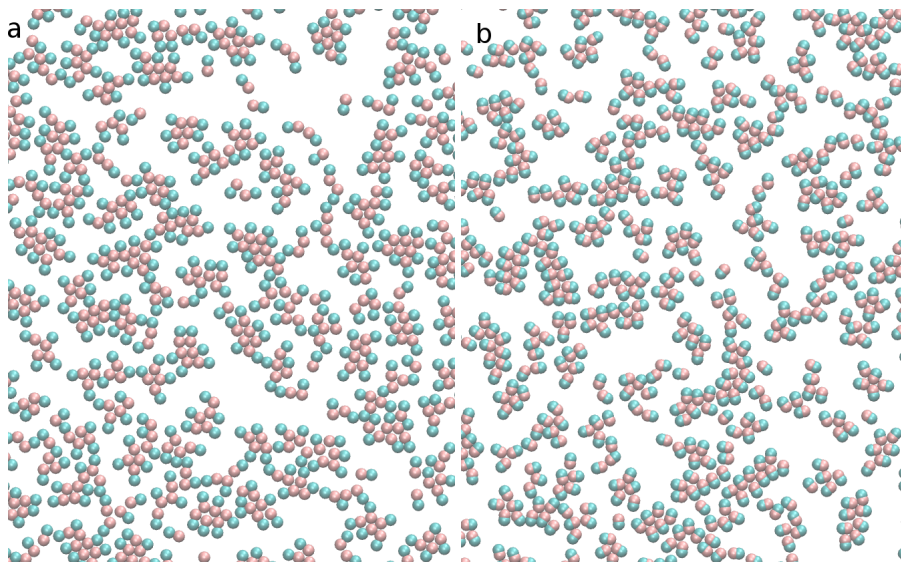


Figure A.9. (Colour online) Snapshot for the system containing only Janus particles. Panel a is for $d^* = 1$, while panel b for $d^* = 0.5$. Snapshots show only a part of the system. The starting density is 0.22 and the temperature is $T^* = 0.4$.

References

1. Fejer S. N., Chakrabarti D., Wales D. J., *Soft Matter*, 2011, **7**, 3553–3564, doi:10.1039/C0SM01289K.
2. Karner C., Dellago C., Bianchi E., *Soft Matter*, doi:10.1039/D0SM00044B, (in press).
3. Xu X., Li Z., Yin Y., *Small*, 2018, **14**, 1801083, doi:10.1002/sml.201801083.
4. Tu F., Park B. J., Lee D., *Langmuir*, 2013, **29**, 12679, doi:10.1021/la402897d.
5. Ao X., Ghosh P. K., Li Y., Schmid G., Hänggi P., Marchesoni F., *Europhys. Lett.*, 2015, **109**, 10003, doi:10.1209/0295-5075/109/10003.
6. Su H., Price A. H., Jing L., Tia Q., Liu J., Qian K., *Mater. Today Bio*, 2019, **4**, 100033, doi:10.1016/j.mtbio.2019.100033.
7. El-Sherbiny I. M., Abbas Y., *Current Pharm. Biotechnol.*, 2016 **17**, 673, doi:10.2174/1389201017666160401145438.
8. Schick I., Lorenz S., Gehrig D., Tenzer S., Storck W., Fischer K., Strand D., Laquai F., Tremel W., Beilstein J. *Nanotechnol.*, 2014, **5**, 2346–2362, doi:10.3762/bjnano.5.244.
9. Gomez-Solano J. R., Blokhuis A., Bechinger D., *Phys. Rev. Lett.*, 2016, **116**, 138301, doi:10.1103/PhysRevLett.116.138301.
10. Feldmann D., Arya P., Lomadze N., Kopyshv A., Santer A., *Appl. Phys. Lett.*, 2019, **115**, 263701, doi:10.1063/1.5129238.
11. Uspal W. E., *J. Chem. Phys.*, 2019, **150**, 114903, doi:10.1063/1.5080967.
12. Huang C., Cheng Y., Zhang H., Wei J., *Part. Part. Syst. Char.*, 2019, **36**, 1970026, doi:10.1002/ppsc.201970026.
13. Amendola V., Meneghetti M., *Nanoscale*, 2009, **1**, 74–88, doi:10.1039/B9NR00146H.
14. Park B. J., Lee D., *Soft Matter*, 2012, **8**, 7690, doi:10.1039/C2SM25775K.
15. Chen D., Amstad E., Zhao C.-X., Cai L., Fan J., Chen Q., Hai M., Koehler S., Zhang H., Liang F., Yang Z., Weitz D. A., *ACS Nano*, 2017, **11**, 11978, doi:10.1021/acsnano.7b03110.
16. Singh V., Cassidy C., Grammatikopoulos P., Djurabekova F., Nordlund K., Sowwan M., *J. Phys. Chem. C*, 2014, **118**, 13869, doi:10.1021/jp500684y.
17. Yoon K., Lee D., Kim J. W., Kim J., Weitz D. A., *Chem. Commun.*, 2012, **48**, 9056, doi:10.1039/C2CC33449F.
18. Bordin J. R., Krott L. B., *Phys. Chem. Chem. Phys.*, 2016, **18**, 28740, doi:10.1039/c6cp05821c.
19. Bordin J. R., Krott L. B., *J. Phys. Chem. B*, 2017, **121**, 4308, doi:10.1021/acs.jpcc.7b01696.
20. Gibbs J. G., Nourhani A., Johnson J. N., Lammert P. E., *MRS Adv.*, 2017, **2**, 3471, doi:10.1557/adv.2017.383.
21. Borówko M., Sokołowski S., Staszewski T., *J. Phys. Chem. B*, 2019, **123**, 5962, doi:10.1021/acs.jpcc.9b04501.
22. Sokołowski S., Pizio O., *Phys. Chem. Chem. Phys.*, 2019, **21**, 11181, doi:10.1039/C9CP01087D.
23. Range G. M., Klapp S. H. L., *Phys. Rev. E*, 2004, **70**, 031201, doi:10.1103/PhysRevE.70.031201.
24. Goyal A., Hall C. K., Velev O. D., *Soft Matter*, 2010, **6**, 480, doi:10.1039/B907873H.
25. Matt B., Pondman K. M., Asshoff S. J., ten Haken B., Fleury B., Katsonis N., *Angew. Chem. Int. Ed.*, 2014, **10**, 12446, doi:10.1002/anie.201404312.
26. Silvera Batista C. A., Larson R. G., Kotov N. A., *Science*, 2015, **350**, 1242477, doi:10.1126/science.1242477.
27. Fan J.-B., Song Y., Liu H., Lu Z., Zhang F., Liu H., Meng J., Gu L., Wang S., Jiang L., *Sci. Adv.*, 2017, **3**, e1603203, doi:10.1126/sciadv.1603203.
28. Kimaev G., *Monte Carlo Simulations of Liquid Crystal-Nanoparticle Mixtures*, MSc. Thesis, University of Waterloo, Waterloo, Ontario, Canada, 2015, <http://hdl.handle.net/10012/9845>.
29. Bouju X., Duguet É., Gauffre F., Henry C. R., Kahn M. L., Mélinon P., Ravaine S., *Adv. Mater.*, 2018, **30**, 1706558, doi:10.1002/adma.201706558.
30. Baran Ł., Borówko M., Rzyśko W., Sokołowski S., *Mol. Phys.*, 2019, **117**, 2802, doi:10.1080/00268976.2018.1554196.
31. Ibenska A., Šimenėnas M., Tornau E. E., *J. Phys. Chem. C*, 2018, **122**, 7344, doi:10.1021/acs.jpcc.8b01828.
32. Szabelski P., Niecekarz D., Rzyśko W., *J. Phys. Chem. C*, **121**, 2017, 25104, doi:10.1021/acs.jpcc.7b06902.
33. Pieranski P., *Phys. Rev. Lett.*, 1980, **45**, 569, doi:10.1103/PhysRevLett.45.569.
34. Hopkins P., Archer A. J., Evans R., *J. Chem. Phys.*, 2009, **131**, 124704, doi:10.1063/1.3212888.
35. Gao H.-M., Lu Z.-Y., Liu H., Sun Z.-Y., An L.-J., *J. Chem. Phys.*, 2014, **141**, 134907, doi:10.1063/1.4897185.
36. Bresme F., Quirke N., *Phys. Chem. Chem. Phys.*, 1999, **1**, 2149, doi:10.1039/A901006H.
37. Frost D. S., Dai L. L., *Langmuir*, 2011, **27**, 11339, doi:10.1021/la202069m.
38. Chung D. L., *J. Chem. Phys.*, 2011, **135**, 054704, doi:10.1063/1.3618553.
39. Ferrara P., Apostolakis V., Caffisch A., *Proteins Struct. Funct. Bioinf.*, 2002, **46**, 24, doi:10.1002/prot.10001.
40. Kamerlin S. C. L., Haranczyk M., Warshel A., *ChemPhysChem*, 2009, **10**, 1125, doi:10.1002/cphc.200800753.
41. Lísal M., Nezbeda I., *Mol. Phys.*, 1999, **96**, 335, doi:10.1080/00268979909482967.
42. Vega C., Paras E. P. A., Monson P. A., *J. Chem. Phys.*, 1992, **96**, 9060, doi:10.1063/1.462214.
43. O’Toole P., Giacometti A., Hudson T., *Soft Matter*, 2017, **13**, 803, doi:10.1039/C6SM02430K.

44. O'Toole P., Munaò G., Giacometti A., Hudson T. S., *Soft Matter*, 2017, **13**, 7141, doi:10.1039/C7SM01401E.
45. Yang Z., Dutt M., Chiew Y. C., *Mater. Res. Express*, 2019, **6**, 075076, doi:10.1088/2053-1591/ab1881.
46. Munaò G., O'Toole P., Hudson T. S., Costa D., Caccamo C., Sciortino F., Giacometti A., *J. Phys.: Condens. Matter*, 2015, **27**, 234101, doi:10.1088/0953-8984/27/23/234101.
47. Munaò G., Costa D., Prestipino S., Caccamo C., *Phys. Chem. Chem. Phys.*, 2016, **18**, 24922, doi:10.1039/c6cp04704a.
48. Munaò G., Costa D., Prestipino S., Caccamo C., *Colloids Surf., A*, 2017, **532**, 397, doi:10.1016/j.colsurfa.2017.04.054.
49. Prestipino S., Munaò G., Costa D., Caccamo C., *J. Chem. Phys.*, 2017, **146**, 084902, doi:10.1063/1.4976704.
50. Borówko M., Rzyśko W., Sokołowski, S., Staszewski T., *J. Chem. Phys.*, 2017, **147**, 014904, doi:10.1063/1.4990415.
51. Borówko M., Rzyśko W., Słyk E., *J. Chem. Phys.*, 2019, **150**, 044705, doi:10.1063/1.5063292.
52. Toxvaerd S., Dyre J. C., *J. Chem. Phys.*, 2011, **134**, 081102, doi:10.1063/1.3558787.
53. Heyes D. M., Okumura H., *Mol. Simul.*, 2006, **32**, 45, doi:10.1080/08927020500529442.
54. Hess S., *Physica A*, 1999, **267**, 58–70, doi:10.1016/S0378-4371(98)00670-0.
55. LAMMPS website, LAMMPS Tutorials, URL <https://lammps.sandia.gov/tutorials.html>.
56. LAMMPS website, Fix langevin command, URL https://lammps.sandia.gov/doc/fix_langevin.html.
57. Rapaport C. D., *The Art of Molecular Dynamics Simulation*, 2nd edition, Cambridge University Press, 2011, doi:10.1017/CBO9780511816581.
58. Chandrasekhar S., *Liquid Crystals*, 2nd edition, Cambridge University Press, 1992.
59. Yankova T. S., Bobrovsky A. Yu., Vorobiev A. Kh., *J. Phys. Chem. B*, 2012, **116**, 6010, doi:10.1021/jp301170b.
60. de Gennes P. G., Prost J., *The Physics of Liquid Crystals*, Clarendon Press, Oxford, 1993.
61. Eppenga R., Frenkel D., *Mol. Phys.*, 1984, **52**, 1303, doi:10.1080/00268978400101951.
62. Rovere M., *J. Phys.: Condens. Matter*, 1993, **5**, B193, doi:10.1088/0953-8984/5/34B/023.
63. Frenkel D., In: *Liquids, Freezing and Glass Transition*, Hansen J. P., Levesque D., Zinn-Justin J. (Eds.), Course 9, Elsevier Science Publishers B.V., 1991, 689–762.

Молекулярно динамічні дослідження двовимірної системи з частинками у вигляді гантелей Януса та сфер

Л. Баран, К. Домбровська, В. Жишко, С. Соколовський

Відділ теоретичної хімії, хімічний факультет університету Марії Склодовської-Кюрі, Люблін 20-031, Польща

Проведено детальне молекулярно динамічне моделювання системи двовимірних частинок у формах гантелей Януса та сфер, що перебувають при постійній температурі. Гантелі Януса моделювались як дві сфери з мітками 1 та 2, з'єднані гармонічними зв'язками. Сфера 1 вибраної гантелі Януса притягує такі самі сфери інших гантелей, тоді як взаємодія між парами 1-1 та 1-2 є відштовхувальною. З іншого боку, сферичні частинки притягуються центрами 2 та відштовхуються силовими центрами 1 частинок Януса. Показано, що структура орієнтованих фаз, які можуть виникати в системі, залежить від довжини зв'язків гантелей Януса та відношення між кількістю сферичних частинок та гантелеподібних. Наявність сферичних частинок є необхідною для появи орієнтованих фаз. Для вибраної моделі формування орієнтованих фаз залежить від концентрації сферичних частинок. Однакова кількість частинок Януса та сфер створює оптимальні умови для формування ламеларних фаз.

Ключові слова: моношари, суміші гантелей Януса та сфер, ламеларні фази, молекулярна динаміка, структурні властивості.